Solar Energy 208 (2020) 894–904

Contents lists available at ScienceDirect

Solar Energy

journal homepage: www.elsevier.com/locate/solener

Stabilization of light-induced effects in Si modules for IEC 61215 design qualification

I.L. Repins [a,*], F. Kersten [b], B. Hallam [c], K. VanSant [d], M.B. Koentopp [b]

[a] National Renewable Energy Laboratory, Golden, CO 80401, USA
[b] Hanwha Q CELLS GmbH, 06766 Bitterfeld-Wolfen, Germany
[c] School of Photovoltaic and Renewable Energy Engineering, University of New South Wales, UNSW Sydney, NSW 2052, Australia
[d] Colorado School of Mines, Physics Dept, Golden, CO 8050, USA

ARTICLE INFO

Keywords:
Photovoltaic reliability
Accelerated testing
IEC 61215
Stabilization
Light induced degradation

ABSTRACT

Standardized testing of commercial photovoltaic modules is widely used around the world and reduces risks of module failures. Such testing also reduces financial risks for module manufacturers and customers. This work examines the expected impact of certain defects in silicon (Si) modules during standardized accelerated testing. Specifically, the behavior of boron-oxygen (BO) light-induced degradation (LID) and light- and elevated temperature-induced degradation (LeTID) are simulated during some of the stress tests in IEC 61215. LID and LeTID reaction rates at qualification temperatures are estimated from earlier published data. It is demonstrated the BO-related LID may cause some false positives and false negatives when IEC 61215 tests are performed as prescribed in the 2016 published version. Possible stabilization steps to avoid these false results are suggested. State changes for the defects causing LeTID occur much more slowly than those causing BO LID, and therefore LeTID is predicted to have a lesser impact on the IEC 61215 stress tests results.

1. Introduction and background

1.1. Module failures and durability

Ensuring that photovoltaic (PV) systems produce the expected energy over their lifetimes is a key factor in the rate at which systems are deployed and generation of solar energy grows. The perceived risk of failures or unexpected degradation plays into insurance rates, finance rates, projected return on investment, and appetite for new spending. When failures occur, they are detrimental to the PV industry, both in terms of decreased return on investment for failure-susceptible products and market spoiling for more robust products. Examples of some high-profile failure types that have been observed in PV systems are fires (Fiorentini et al., 2016), potential-induced degradation (Yang et al., 2017), backsheet cracking (Pickerel 2020), and LeTID (Deceglie et al., 2020; Kersten et al., 2017).

Finely tuned accelerated testing is the key to minimizing the occurrence of module failures in PV systems, and distinguishing between high-risk and low-risk products. Since the 1970′s, accelerated tests for PV module reliability have been developed by applying stresses (such as heat, light, and humidity) in a manner that reproduces observed failures of fielded modules in a laboratory test of reasonable duration (Osterwald et al., 2009; Smokler et al., 1985; Wohlgemuth, 2011). The use of accelerated tests for PV module durability has been extremely successful. In one of the earliest large studies of PV module reliability (Ross et al., 1986), the iterative process of creating accelerated tests based on observed failures, then modifying module design to pass the new tests, increased average PV module lifetime from one year to over ten years. Today, the process of accelerated testing for improved module durability continues. At present, the typical warranty for PV modules is 25 years, and extended warranties are 30 years.

Correctly setting test procedures and stress levels in accelerated tests is a key element of this success. If tests are too easy, deployed module failures are likely to occur, affecting consumer confidence. If test levels are too harsh, they can constrict the industry by requiring costly additions to the module design, or by needlessly failing promising new technologies. Test procedures and stress levels are the subject of continued effort, as degradation mechanisms may manifest in different ways with changes in technology and lengthening of the expected module service life.

* Corresponding author.
E-mail address: ingrid.repins@nrel.gov (I.L. Repins).

https://doi.org/10.1016/j.solener.2020.08.025
Received 30 June 2020; Received in revised form 7 August 2020; Accepted 10 August 2020
Available online 26 August 2020

1.2. IEC 61215

The accelerated tests in the IEC 61215 (IEC, 2016) international standard series (for module durability) are widely used around the world for requirements in electrical and building codes, incentive programs, and purchasing agreements. An introduction to the IEC 61215 series is given here, since this manuscript considers how recent developments in PV module designs impact IEC 61215 test result interpretation, and how such tests – particularly stabilization procedures - should be revised to continue to deliver the most meaningful results.

IEC 61215 series accomplishes photovoltaic (PV) module design qualification, i.e. it determines if modules of a given design are likely to experience known failures out in the field. Modules are subjected to performance characterization and a variety of accelerated stress tests which have been empirically developed to separate failed or degraded populations of modules from those that performed to expectations (Ross et al., 1986; Runkle et al., 1980). Examples of accelerated stress tests applied during IEC 61215 testing are damp heat (DH), mechanical load (ML), and thermal cycling (TC). IEC 61215 testing delivers a "pass" or "fail" designation to a set of modules. Some of the requirements for a "pass" are based on module performance. First, the initial module performance must match the module label. This comparison is known as "Gate 1". After the accelerated stress tests, the module must retain 95% of its initial power generation. This comparison is known as "Gate 2".

Evaluation of Gate 1 and Gate 2 requires proper module stabilization. Such stabilization includes, for example, putting metastable states in CIGS and CdTe modules into a reproducible and field-representative configuration (Deceglie et al., 2015), effecting the initial rapid Staebler-Wronski degradation in amorphous Si modules (Mateo et al., 2018; Kenny et al., 2014), or causing defect states related to BO LID or LeTID to progress to a field-relevant condition (Niewelt et al., 2017; Pingel et al., 2010; Lee et al., 2015). Without proper stabilization, a module's performance may appear either too high or too low, depending on the module's starting state, the mechanism causing the instability, and the stabilization procedure being used. Thus, without proper stabilization, pass/fail designations from Gate 1 or Gate 2 may be erroneous.

1.3. Light-induced effects requiring stabilization in crystalline Si modules

BO LID and LeTID pose new challenges in accelerated testing. Customers have been willing to pay a premium for higher efficiency modules that improve return on investment via decreased balance-of-system costs (such as installation, racking, permitting, and land costs) (Peters et al., 2019; Chang et al., 2018). This drive toward higher-efficiency modules has implications for light-induced effects and accelerated testing. First, higher efficiencies depend partially on longer minority carrier lifetimes. Since BO LID and LeTID are associated with bulk recombination centers, their impact is expected to be largest in high-efficiency devices, compared to less-efficient devices where minority carrier lifetime is already limited by other types of defects. Second, the desirability of higher efficiencies has caused the market share of monocrystalline Si to increase in recent years (Colville, 2017). The relatively high concentrations of oxygen in Czochralski-grown monocrystalline Si increase the potential concentration of BO defects. Third, a significant number of manufacturers are maximizing nameplate efficiency by performing procedures involving carrier injection (Lee et al., 2015; Hallam et al., 2018) to put light-sensitive defects into a regenerated state. However, some testing conditions may change the state of defects in a way that is not representative of field behavior and is not related to the degradation mechanisms targeted by the stress test. Thus, accelerated tests that unintentionally destabilize such defects (Kersten et al., 2019) may require modification. Finally, while manufacturers may introduce more hydrogen (H) into devices to more fully regenerate BO defects (Hallam et al., 2018) and thus achieve higher efficiency, the increased H may also lead to a larger extent of LeTID (Bredemeier et al., 2019).

While several types of defect complexes can cause light-induced performance changes in crystalline Si, BO LID and LeTID are of primary concern because they can occur with a greater than 5% effect on power output in modern PV modules, greatly impacting the long-term energy yield. Since BO LID and LeTID may occur in parallel with each other, and with other degradation mechanisms, the Gate 2 requirement of 95% performance retention requires that even effects causing 1 to 2% changes are treated thoroughly, so that the pass/fail designation is accurate.

Some limited background on BO LID and LeTID is provided very briefly in order to summarize the key characteristics that are important to IEC 61215 stabilization. BO LID primarily affects *p*-type Czochralski (Cz) solar cells due to the high concentrations of both boron and oxygen in the Si material (Bothe et al., 2005). LeTID can affect both multicrystalline and Cz Si solar cells. Some early research shows that LeTID may also occur in *n*-type Si (Chen et al., 2018; Sio et al., 2018). Under module operating conditions, both BO LID and LeTID progress from an initial state (highest power), to a degraded state (lower power), and finally to a regenerated state (power equal to, or nearly equal to, the initial state). For both effects, this progression is accelerated by higher temperatures and increased carrier injection. There are numerous published works relating to the kinetics (i.e. reaction rates) of BO LID (Glaser et al., 2015; Helmich et al., 2018; Sun et al., 2019; Herguth et al., 2010; Bothe et al., 2006; Wilking et al., 2014; Steckenreiter et al., 2017; Herguth et al., 2008; Graf et al., 2019; Hallam et al., 2016) but fewer relating to the that of LeTID (Bredemeier et al., 2017; Graf et al., 2019; Jensen et al., 2017; Kwapil et al., 2017; Payne et al., 2016; Fokuhl et al., 2019; Vargas et al., 2019; Herguth et al., 2017). For BO LID, the initial, degraded, and regenerated states are typically referred to as "A", "B", and "C", respectively, as illustrated in Fig. 1. That naming convention will be followed in this paper. In Fig. 1, the direction in which reactions progress with carrier injection (i.e. with light or current) are shown as black arrows. The black arrows also represent the net direction of reactions under fielded conditions, since the highest temperatures (which accelerate reactions) occur when sunlight is present. The cross-hatched gray arrows show the progression during some accelerated tests where heat is applied without carrier injection. Examples of such tests include the IEC 61215 damp heat or humidity-freeze stress tests.

The names for transitions between the states shown in Fig. 1 are referred to using the terminology defined for BO LID in earlier references (Wilking et al., 2015). Specifically, transitions from A to B are termed "degradation," those from B to C are "regeneration", those from C to B are "destabilization," and those from B to A are "annealing." Some works have referred to "destabilization" as the transition from C to B to A (Hieslmair et al., 2017). These two definitions of "destabilization" found in the literature are somewhat consistent, since BO defects in state A can

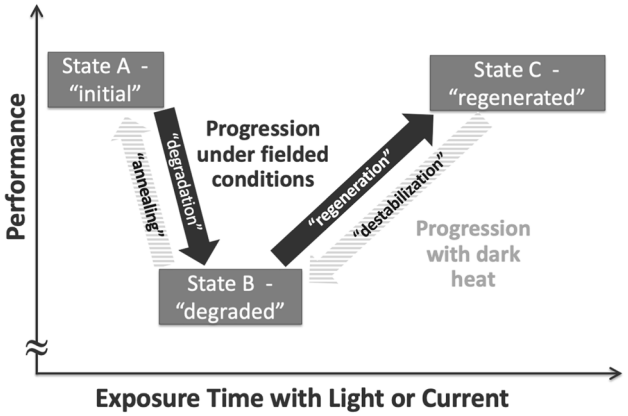

Fig. 1. Schematic illustration showing progression of module performance when BO LID occurs.

transition to state B relatively quickly with a short room-temperature light soak. In this work "destabilization" refers to the transition from state C to state B.

Although BO LID and LeTID can both follow a progression from an initial, via degraded, to a regenerated state, there are several differences between the kinetics of the effects. First, for conditions encountered by fielded modules or in IEC 61215 accelerated tests, BO LID progresses much more quickly than LeTID. Second, while dark heat can cause BO LID states to change in the direction opposite from that encountered in fielded modules (gray arrows in Fig. 1), observations of such transitions for LeTID are limited. One study (Herguth et al., 2017) deduces that a transition from the LeTID degraded state to the initial state may occur above 200 °C which is far outside field-relevant temperatures. Transitions from the LeTID regenerated state to the degraded state have not yet been reported in the literature. Third, at elevated temperatures, LeTID may progress along the black arrows in Fig. 1 without light or current injection (Vargas et al., 2019; Liu et al., 2018; Luka et al., 2018; Chen et al., 2017). The rate of dark LeTID reactions at qualification test temperatures (≤85 °C) is slow compared to those of other transitions considered in this work (see Table 1 and following).

1.4. General methodology

The goal of this study is to define updates to IEC 61215 that ensure meaningful accelerated test procedures for commercial PV modules. A significant inherent challenge is that qualification tests are being used continuously on commercial products, regardless of whether the compatibility of the existing tests with new product designs has been evaluated or understood. In some cases, standardized misinterpretation of BO LID or LeTID artifacts affects the pass-fail status of these products. Thus, test procedures must be updated immediately based on the best-available current data and understanding. When more comprehensive and rigorous data sets are available in the future, test procedures will again be refined.

The general methodology used in this study is shown in Fig. 2. Each box in the figure represents one step in the process. Where appropriate, text in parentheses identifies where in this paper that step is discussed or summarized. Black arrows show the order in which steps are executed. The first stage of the method is to define relevant defect properties as well as the conditions encountered during IEC 61215 stress tests. This stage is marked as "Definitions" on the left side of Fig. 2, and includes the top two boxes in the flow chart. The second stage is marked as "Choice of Conditions" in Fig. 2. In this stage, one stress condition and one defect starting state are chosen from the definitions of the previous stage, in order to represent one stress test on one product. For example, as shown on the right side of Fig. 2, one might choose to simulate the effect of 200 thermal cycles on a module with defects that cause LeTID and are in the initial state. Next, calculations are performed, as marked to the left of the fourth and fifth boxes. The change in the population of various defect states with applied stress is calculated. This calculation yields the percent of defects that are in the initial, degraded, or regenerated state, as shown in the example on the right side of Fig. 2. The change in defect populations with time is non-linear, since the calculation takes into account both the reaction rate and the number of available defects. The population of the defects states is then used to calculate the power output change from the module (second graph in Fig. 2). By repeating these calculations for each stress in IEC 61215 and each defect variation, one can estimate the possible impact of BO LID and LeTID on test results and recommend updates to the testing procedure. The next sections detail the inputs to and execution of the steps in Fig. 2.

2. Simulation inputs

This work utilizes rate constants either presented in earlier experimental studies or derived from the data of those studies. These rate constants are needed to estimate the effect of BO LID and LeTID on accelerated stress tests in IEC 61215:2016, and to assess the impact of an added stabilization step. (Consistent with IEC notation, "IEC 61215:2016" is used when specifically referring to the version of the test procedures published in 2016, whereas "IEC 61215" is used to refer to any version, such as when discussing the purpose of the standard, or possible revisions for future editions.)

2.1. Summary of parameters

Table 1 summarizes the parameters used in this work to simulate how BO LID or LeTID may change the results of IEC 61215 stress tests. The table lists, in the first two columns, the degradation mechanism (BO LID or LeTID), and each transition between states. The remaining columns show, for each entry, the kinetic constants. For kinetic constants that vary with illumination, the fourth column shows the injection level at which the measured values were obtained, in units of suns at open circuit. Rates are described in terms of the attempt frequency (ν) and activation energy (E_a). The reaction rate (k), for any transition is derived from ν and E_a and is assumed to follow the typical Arrhenius equation, (Laidler, 1984)

$$k = \nu e^{-E_a/k_B T} \quad (1)$$

where k_B is Boltzmann's constant and T is the temperature in Kelvin. The resulting set of differential equations that quantify the transition of defects between A, B, and C are written out explicitly for BO LID in other

Table 1
Parameters used in the simulation of BO LID and LeTID at 85 °C based on published reaction rates in the literature.

Mechanism	Transition	Published attempt frequency, ν (s^{-1})	Injection level at which ν was measured (Suns[†])	Published activation energy, E_a (eV)	Resulting rate (k) at 85 °C, 1 Sun (s^{-1})	Reference
BO LID	A to B	$4 \cdot 10^3$	Not applicable	0.475 ± 0.035	$8.18 \cdot 10^{-4}$	(Bothe et al., 2006; Hallam et al., 2016)
	B to A	$1 \cdot 10^{13}$	0	1.32 ± 0.05	$2.58 \cdot 10^{-6}$	(Bothe et al., 2006; Hallam et al., 2016)
	B to C	$1.25 \cdot 10^{10}$	2.7	0.98 ± 0.06	$7.32 \cdot 10^{-5}$	(Wilking et al., 2014; Hallam et al., 2016)
	C to B				$2.8 \cdot 10^{-7}$	(Kersten et al., 2019), See section 2.3
LeTID	Initial to Degraded	$9.37 \cdot 10^8$	0.5	0.94	$1.08 \cdot 10^{-4}$	(Bredemeier et al., 2017)
	Degraded to Regenerated				$1.2 \cdot 10^{-6}$	(Kersten et al., 2015), See section 2.4
LeTID (Dark)	Initial to Degraded	$8.44 \cdot 10^7$	0	1.08	$5.21 \cdot 10^{-8}$	(Vargas et al., 2019)
	Degraded to Regenerated	$1.79 \cdot 10^7$	0	1.11	$4.18 \cdot 10^{-9}$	(Vargas et al., 2019)

[†] Units of suns are used here following the typical definition: One sun is 1000 W/m^2 of AM1.5 spectrum.

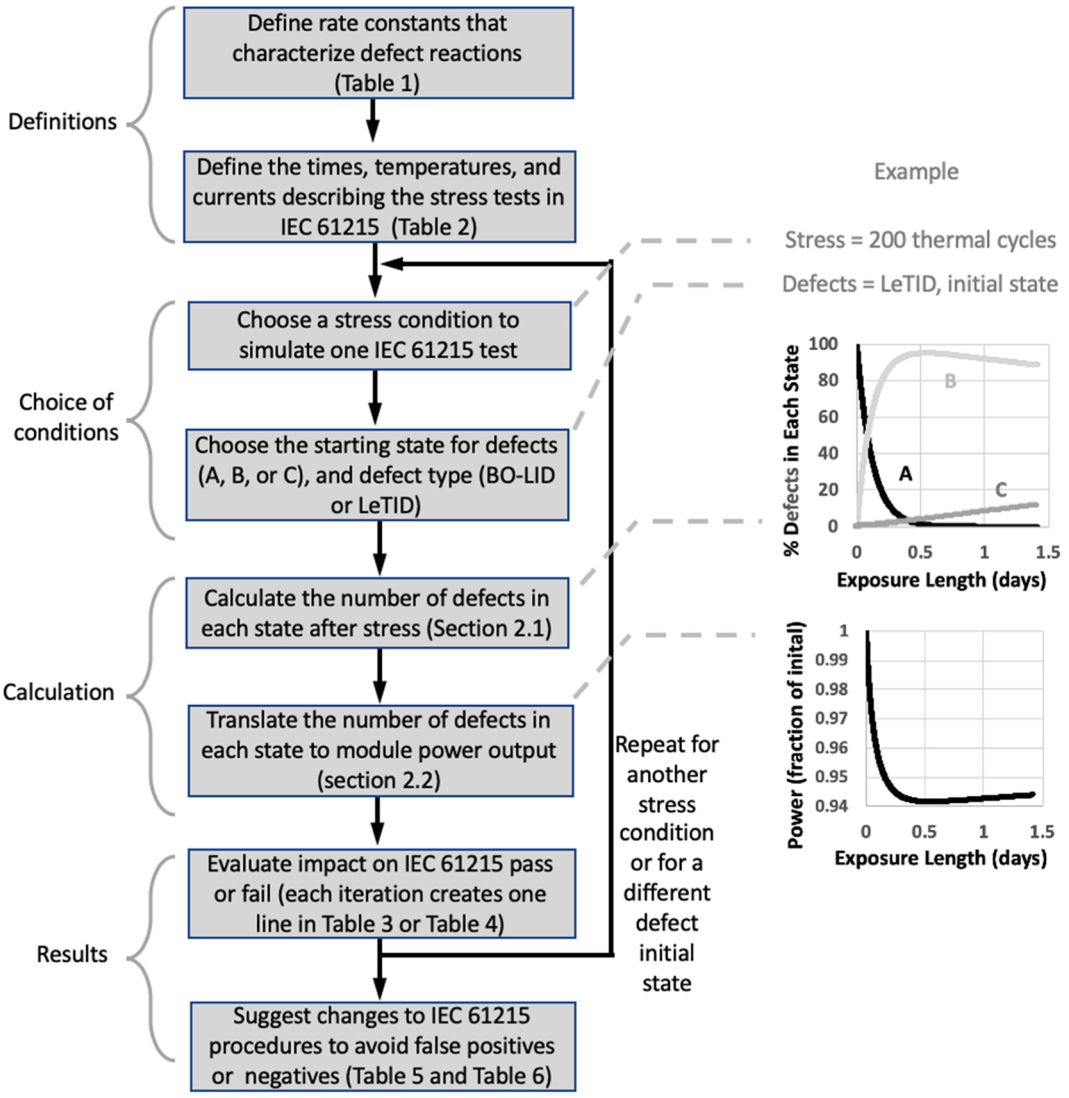

Fig. 2. Flow chart illustration of the methodology applied in this study. Black arrows show the order for executing the steps. Text in parentheses describes where in this paper that step is discussed or summarized. The right side shows an example of the output of four steps.

works (Herguth et al., 2010; Hallam et al., 2016). Table 1 also lists the reaction rate that results from evaluating Eq. (i) at 85 °C (the highest temperature used in IEC 61215 tests) for each transition. The final column in Table 1 references the published data that were used to specify values for ν and E_a for that transition. In most cases, the values were taken directly from the published work, so the final column only refers to the cited studies. In two cases, deriving a reaction rate uses data from the cited studies, but some fitting is performed in this paper. In those cases, the final column cites the studies providing the experimental data, and also the section of this paper in which the fitting is performed and discussed. For LeTID, Table 1 does not list parameters for defect annealing, or defect destabilization, since these reactions have not yet been observed at the relatively low temperatures (≤85 °C) used during IEC 61215 qualification tests or encountered in typical field conditions.

Carrier injection dependency is included in the treatment of Table 1 parameters where applicable. For BO LID, the regeneration rate has been shown to be linear with injected carrier density (Steckenreiter et al., 2017). Thus, in simulating BO LID, the reaction rate k for the transition from B to C scales with carrier injection. Similarly, LeTID degradation and regeneration processes have been observed to be accelerated with carrier injection (Kwapil et al., 2017; Kersten et al., 2015) and k is scaled accordingly. In other words, for processes that accelerate with carrier injection, the attempt frequency used in the simulation of a given stress (k_{stress}), is taken to be the 1-sun attempt frequency of Table 1 (k_1) by ratio of the current injected during stress (I_{stress}) versus to that injected under 1-sun conditions (I_{sc}):

$$k_{stress} = k_1 \cdot \frac{I_{stress}}{I_{sc}} \quad (2)$$

For BO LID degradation, it has been shown that the degradation rate is roughly independent of illumination (i.e. carrier injection) for intensities greater than 0.01 sun (Hashigami et al., 2003). Thus, the attempt frequency for the BO LID degradation process is taken as fixed with respect to carrier injection for these simulations. It has been demonstrated that carrier injection via illumination or the application of current are equivalent for accelerating LeTID degradation (Payne et al., 2016; Kersten et al., 2015), LeTID regeneration (Kersten et al., 2015), BO LID degradation (Knobloch et al., 1996; Glunz et al., 2003), and BO LID regeneration (Herguth et al., 2006; Lin et al., 2017). Thus, no distinction is made in the simulation between light versus dark stress exposures – in either case the magnitude of the injected current is used to perform scaling of attempt frequencies.

The entries in Table 1 are only approximate values used to estimate effects during module qualification. Some effects are ignored. First, kinetic parameters are likely to depend on cell properties. For example, it has been observed that the BO regeneration rate depends on the B

concentration (Lim et al., 2009). Also, while equation ii describes a simple linear correction to attempt frequencies for reactions that are accelerated by carrier injection, some work has documented a quadratic dependency (Wilking, 2017). Finally, the effect of evolving minority carrier lifetime on excess carrier density for a fixed injection level (Graf et al., 2019) is ignored. Instead, kinetic constants are applied the same way they are derived (Bredemeier et al., 2017; Wilking et al., 2014), which is without correction for changing minority carrier lifetimes during the degradation and recovery cycle.

2.2. Translation between defect state and power loss

The parameters in Table 1 allow quantification transition rates between defect states for a given starting condition, with exposure to specific temperatures and current injection levels for known times. Thus, the information obtained from Table 1 is what percentage of defects are in the initial, degraded, or regenerated states after a given stress procedure. However, IEC 61215 Gate 1 and 2 evaluate the module in terms of power. Thus, in order to understand how the defect transitions impact module qualifications, it is necessary to convert the defect status into an approximate effect on the module performance. To accomplish this conversion, the lifetime and the activated BO defects are treated in the manner detailed by Glunz et al. (2003) and others. To summarize, the total minority carrier lifetime, τ, is broken into two components: τ_{BO} which is the carrier lifetime due to activated (state B) BO defects, and τ_{res}, which is the lifetime due to all other recombination mechanisms. τ_{BO} is inversely proportional to the fraction of BO defects that are in the degraded state. The components of the minority carrier lifetime combine in the usual manner, i.e.

$$\frac{1}{\tau} = \frac{1}{\tau_{BO}} + \frac{1}{\tau_{res}} \quad (3)$$

and the open-circuit voltage (V_{oc}) depends on the natural log of the total carrier lifetime. Some work has assumed power output is proportional to V_{oc} (Müller et al., 2018), for simplicity ignoring the typical correlation between fill factor *FF* and V_{oc}, as well as any impact on the short-circuit current. This work includes one further refinement beyond Müller et al. (2018): An empirical expression is used to derive *FF* from V_{oc} (Green, 1982). The change in power is then calculated from the change in the product of *FF* and V_{oc}. The same method is used to convert between defect populations and power output for LeTID.

In the examples of expected changes during IEC 61215 stress that are presented later, initial and degraded lifetimes are chosen to replicate a 6% degradation due to BO LID or LeTID. A 6% degradation is representative of some of the larger, though not anomalous, changes that have been observed in modules (Ramspeck et al., 2012). Initial cell voltage is also taken from Ramspeck et al. (2012). In general, the magnitude of the effect varies depending on cell characteristics and processing.

2.3. BO LID destabilization rate

Literature values for BO LID destabilization attempt frequency and activation energy are not used in Table 1. Recent reports from test labs and publications (Hieslmair et al., 2017; Kersten et al., 2019; Fertig et al., 2014) suggest that commercial cells and modules undergo substantial BO LID destabilization during the 1000 h at 85 °C encountered during IEC 61215 damp heat testing. However, if one utilizes literature values for BO destabilization (Wilking et al., 2014), one would predict only 5% destabilization (e.g. a regenerated module that would experience 6% relative power loss with complete destabilization would be predicted to experience only 6% × 0.05 = 0.3% relative power loss in DH testing). It is likely that the earlier literature values of kinetic parameters for BO destabilization included contributions from surface passivation (Wilking et al., 2014), leading to activation energies higher than recently observed. Extrapolation of the rates from the higher temperatures used to derive E_a and ν (170–245 °C) (Wilking et al., 2014) to the lower temperatures used in qualification tests thus predict a very low reaction rate.

Based on recent reports of destabilization during module qualification testing, the destabilization rate was reconsidered. The data points in Fig. 3 show measured performance change as a function of time at 85 °C in the dark. The data are taken from Fig. 4 in Kersten et al. (2019), where the performance change is shown to be due to BO destabilization. In order to derive a reaction rate, k, from these data, the fraction of BO defects in the degraded state as a function of time was calculated, with k as a variable. The defect populations were converted to change in power, using the method described in Section 2.b. k was then varied to perform a least squares fit, shown as the dotted line in Fig. 3. The fit yields a reaction rate of $2.8 \cdot 10^{-7}\ s^{-1}$. This reaction rate for BO destabilization is included in Table 1 and is used for calculations in this work.

Experiments have shown that regenerated BO LID defects will not destabilize in field conditions, even with extended periods of dark storage in hot climates (Kersten et al., 2019). Thus, test procedures should be designed such that the destabilization process depicted in Fig. 3 does not affect the module's qualification status. Of particular concern are stress tests at elevated temperatures that do not provide illumination or current injection.

2.4. LeTID reaction rates

LeTID has only been observed relatively recently: First observations of LeTID were published in 2012 (Ramspeck et al., 2012), compared to the 1970's (Fischer et al., 1973) for BO LID. Thus, LeTID degradation and regeneration have not yet been studied as thoroughly as the corresponding processes in BO LID. Paired attempt frequency and activation energy value have not yet been published to describe LeTID regeneration.

Some data from Kersten et al. (2015) are therefore fitted to provide a LeTID regeneration rate at 85 °C. The data points in Fig. 4 show measured performance change as a function of time exposed to 85 °C with injected current. These points represent LeTID regeneration of four different modules. Data were taken under conditions with current injection equivalent to 1-sun open-circuit: either at open-circuit under one-sun illumination, or in the dark with the one-sun short-circuit current (I_{sc}) applied to the module terminals. A least-squares fit of the data yields a regeneration reaction rate of $1.2 \cdot 10^{-6}\ s^{-1}$. The fit models the portion of the regeneration that was attributed to LeTID in the earlier study. The derived reaction rate for LeTID regeneration is included in Table 1 and is used for calculations in this work.

In this work, for estimating effects from LeTID, the degradation

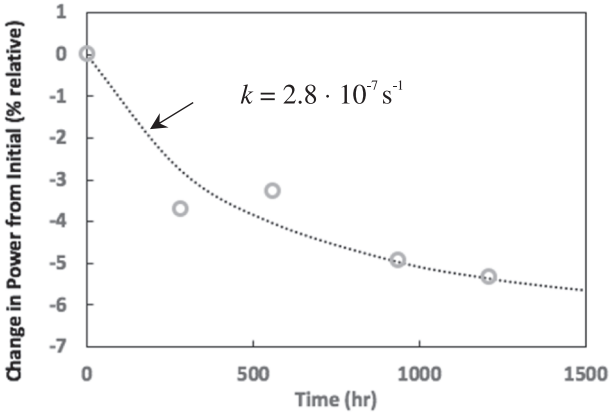

Fig. 3. Open circles are BO-LID destabilization data from Kersten et al. (2019), Fig. 4. Least squares fit (dotted line) yields a reaction rate of $2.8 \cdot 10^{-7}\ s^{-1}$ at 85 °C.

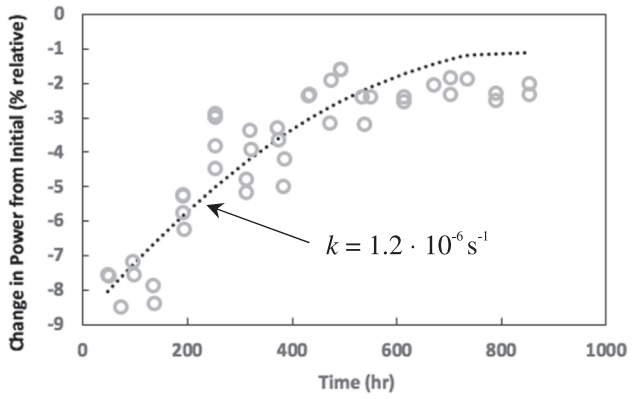

Fig. 4. LeTID regeneration data with reaction rate fit. Data points are taken from Fig. 6 in Kersten et al. (2015).

constants derived by Bredemeier et al. (2017) are used. It should be noted that there is considerable variation in LeTID degradation rates reported across the literature. Using the Bredemeier constants, 80% of LeTID degradation is predicted to occur in ~ 50 h, for a module at 85 °C with I_{MPP} injected current. However, another study (Kersten et al., 2015) (performed under the same conditions) observed 80% of LeTID degradation occurring in ~ 300 h. A number of factors may play into the disagreement. Long minority carrier lifetime may accelerate the LeTID due to the dependence of the reaction rates on injection level. For a fixed injected current, samples with longer carrier lifetime should maintain a higher carrier density, allowing degradation to occur faster (Graf et al., 2019). Also, some samples may exhibit more than one degradation mechanism occurring in parallel, which influences the extraction of kinetic parameters (Graf et al., 2019). Variations in the time scale of LeTID have been observed across products, but have not yet been associated with a specific cell property (Fokuhl et al., 2019). The LeTID degradation rates utilized in this study represent the faster end of those observed in experiment.

3. Simulation results

The parameters in Table 2 are used to estimate how BO LID and LeTID may impact the results of IEC 61215 qualification tests.

3.1. Stress conditions

Tests where light-induced effects were observed to have an impact were 200 TC (sequence D in IEC 61215:2016), DH (sequence E in IEC 61215:2016), and 50 thermal cycles followed by 10 humidity-freeze (HF) cycles (sequence C in IEC 61215:2016). Potential induced degradation (PID) stress, as described in IEC 62804-1 and planned for the IEC 61215 new edition (2020 estimated publication), was also simulated. For stresses that involve temperature cycles, only the times at highest temperature were used for simulation due to the high activation energies of the reactions. The IEC 61215 stresses and the simplified parameters used for simulation are summarized in Table 2. Where the test prescribes applying maximum power current, the applied current is estimated to be 90% of the one-sun I_{sc}. The current input to the simulation (sixth column in Table 2) scales the 1-sun attempt frequencies for the injection-dependent processes in Table 1.

3.2. Impact on IEC 61215:2016 results

Table 3 shows simulation results for a module that exhibits 6% BO LID but no other degradation mechanisms. Thus, any changes in power (deviations from 100% relative) that are indicated in the table are caused by BO LID defects changing states. The table columns show BO LID defect states, applied stresses, and power measurements, in chronological order from left to right. Applied stresses are abbreviated as TC, DH and HF. Also included in Table 3 is the short, low-temperature light soak (named "MQT 19.1" in IEC 61215), which is required before the first power measurement. Manufacturers may ship modules in the initial (A), degraded (B), or regenerated (C), states, so the row for each stress sequence is subdivided to show results for each possible starting state. Where BO LID defect state has more than a 2% effect on apparent power, numbers are highlighted in large bold text. Parentheses are used to indicate variability introduced by the BO LID defects. During storage under room lights, the initial state A can degrade toward state B in measurable amounts over the course of minutes. Thus, depending on how the module is handled between stress and characterization, a given lab may obtain any value ranging from the one in parentheses (if all state A defects degrade to B) to the one outside the parenthesis. The vertical arrows at the bottom of the table show the location in each stress sequence where Gate 1 or Gate 2 power measurements are performed.

According to Table 3, BO LID combined with the current IEC 61215 test protocol may contribute to both false positives (modules that pass when they should not) and false negatives (modules that fail when they should not). A module that experiences, for example, 6% power decrease due to solder bond failures with 200 thermal cycles should fail Gate 2. If, however, this real power decrease is offset by a 6.3% power increase from BO LID state changes (as in the first row of Table 3), then the module will pass Gate 2. Likewise, a module that degrades only 2% under damp heat due to resistance changes in cell materials should pass Gate 2. Such a module may be delivered with BO LID defects in the regenerated state, which are then destabilized during DH stress. The 2% actual degradation, plus an apparent 3.5% decrease due to destabilization of the BO defects (ninth row of Table 3), can cause the module to fail Gate 2.

The analogous calculations are applied to LeTID. Table 4 shows simulation results for a module that exhibits 6% LeTID but no other degradation mechanisms. LeTID progresses more slowly than BO LID, and only advances significantly (in this time and temperature range) with applied current. Of the stress tests considered in this paper, current is applied only during thermal cycling. At thermal cycle test conditions, the transition from the initial to degraded state is much faster than that from the degraded to the regenerated state. Thus, the impact of LeTID on

Table 2
IEC 61215 stress tests that may be affected by light-induced defects, and the simplified parameters used for simulation.

	IEC Stress			Simulation Input		
Stress (IEC 61215 sequence)	**Critical conditions**	**Time**	**Current**	**Temp. (°C)**	**Current (% of I_{sc} at 1 sun)**	**Time (days)**
50 Thermal Cycles (C)	Each cycle has 10-minute minimum dwell time at highest temperature of 85 °C	10 min × 50 cycles = 8.3 h	Maximum power current	85	90	0.4
10 Humidity Freeze Cycles (C)	Each cycle has 20-hour minimum dwell time at highest temperature of 85 °C	20 h × 10 cycles = 200 h	0	85	0	8.3
200 Thermal Cycles (D)	Each cycle has 10-minute minimum dwell time at highest temperature of 85 °C	10 min × 200 cycles = 33.3 h	Maximum power current	85	90	1.4
Damp heat (E)	85 °C	1000 h	0	85	0	41.7
PID (F planned)	85 °C	96 h	0	85	0	4.0

Table 3
Simulated defect status and apparent performance change for a module that exhibits 6% BO LID and no other degradation, for portions of the IEC 61215:2016 test protocol.

At right is each step as module advances through the sequence:	BO defect starting state	Defect status after MQT 19.1	Stress 1	Defect status following stress 1	Stress 2	Defect status following stress 2	Final power, relative to Gate 1 (%)
IEC 61215 Sequence C	A	B	50 TC	90% C, 10% B	10 HF	73%C, 18%A, 9%B	(**103.7** to) **105.3**
	B	B	50 TC	90% C, 10% B	10 HF	73%C, 18%A, 9%B	(**103.7** to) **105.3**
	C	C	50 TC	1% B, 99% C	10 HF	11% A, 8%B, 81%C	(98.1 to) 99.1
IEC 61215 Sequence D	A	B	200 TC	99% C,1% B	–	–	**106.3**
	B	B	200 TC	99% C, 1% B	–	–	**106.3**
	C	C	200 TC	99% C, 1% B	–	–	100
IEC 61215 Sequence E	A	B	DH	A	–	–	(100 to) **106.4**
	B	B	DH	A	–	–	(100 to) **106.4**
	C	C	DH	36% C, 5% B, 59% A	–	–	(**96.5** to) 99.5
IEC 61215 Sequence F (planned)	A	B	PID	59% A, 41% B	–	–	(100 to) **102.7**
	B	B	PID	59% A, 41% B	–	–	(100 to) **102.7**
	C	C	PID	91% C, 6% B, 3% A	–	–	(99.0 to) 99.3
		↑ Gate 1 Measurement				↑ Gate 2 Measurements	

Table 4
Simulated defect status and apparent performance change for a module that exhibits 6% LeTID and no other degradation, for portions of the IEC 61215:2016 test proceeding.

At right is each step as module advances through the sequence:	LeTID defect starting state	LeTID defect status after MQT 19.1	Stress 1	LeTID defect status following stress 1	Stress 2	Defect status following stress 2	Final power, relative to gate 1 (%)
IEC 61215 Sequence C	Initial	Initial	50 TC	3% initial, 94% degraded, 3% regenerated	10 HF	3% initial, 94% degraded, 3% regenerated	**94.2**
	Degraded	Degraded	50 TC	96% degraded, 4% regenerated	10 HF	96% degraded, 4% regenerated	100.1
	Regenerated	Regenerated	50 TC	100% regenerated	10 HF	100% regenerated	100
IEC 61215 Sequence D	Initial	Initial	200 TC	89% degraded, 11% regenerated	–	–	**94.4**
	Degraded	Degraded	200 TC	88% degraded, 12% regenerated	–	–	100.4
	Regenerated	Regenerated	200 TC	100% regenerated	–	–	100
IEC 61215 Sequence E	Initial	Initial	DH	83% initial, 17% degraded	–	–	98.2
	Degraded	Degraded	DH	99% degraded, 1% regenerated	–	–	100
	Regenerated	Regenerated	DH	100% regenerated	–	–	100
IEC 61215 Sequence F (planned)	Initial	Initial	PID	100% initial	–	–	100
	Degraded	Degraded	PID	100% degraded	–	–	100
	Regenerated	Regenerated	PID	100% regenerated	–	–	100
		↑ Gate 1 Measurement				↑ Gate 2 Measurements	

thermal cycling tests is largest for modules starting in the initial state. The first and fourth rows of Table 4 indicate that a substantial fraction of LeTID degradation may occur during thermal cycling for samples starting in the initial state. Since LeTID is in fact a process that causes long-term power degradation in fielded modules, it may be acceptable that LeTID can contribute to a TC qualification failure. Furthermore, LeTID will not cause false positives. Thus, the need for revision of IEC 61215 test procedures (in order to avoid false positives or fails) is motivated primarily by effects related to BO LID, rather than LeTID. The urgent revision is, therefore, of most importance for *p*-type Cz material (Bothe et al., 2005), which is increasing in market share.

The IEC 61215 stress tests do not quantify LeTID or BO LID. Thus, a separate procedure should be developed to separate and measure each of these light-induced effects and provide guidance on how the measured values are expected to impact energy yield.

3.3. Strategies for improved stabilization

The need for improved stabilization procedures in the IEC 61215 test protocol is implied by the possibility of both false positive and false negative test results, as discussed earlier related to Table 3.

An improved stabilization, applying I_{sc} to the module in the dark for 48 h at 85 °C, is proposed. An earlier study verified experimentally that the application of approximately these conditions was sufficient to put all BO defects into the regenerated state, and reverse unintentional destabilization that occurs during DH testing (Kersten et al., 2019). Calculations confirm these experiments. Calculations in Fig. 5 shows the percent of states that are regenerated during a 48-hour stabilization treatment involving elevated temperature and application of I_{sc}. The calculation was performed using the kinetic parameters from Table 1, for a sample starting in the initial state. Calculations are shown over the temperature range of 25 °C to 85 °C. For the 85 °C stabilization (solid black curve), 99% of the defects are already regenerated after one day. Thus, the proposed stabilization conditions are conservative: They allow for more than enough time to regenerate the module, even if there is some variation in kinetic constants or experimental conditions.

The improved stabilization is required both before and after stress: Any stabilization that can reverse non-field representative destabilization (i.e. avoiding a false negative after DH for a module that starts in state C) will also drive modules with defects in state B to regeneration,

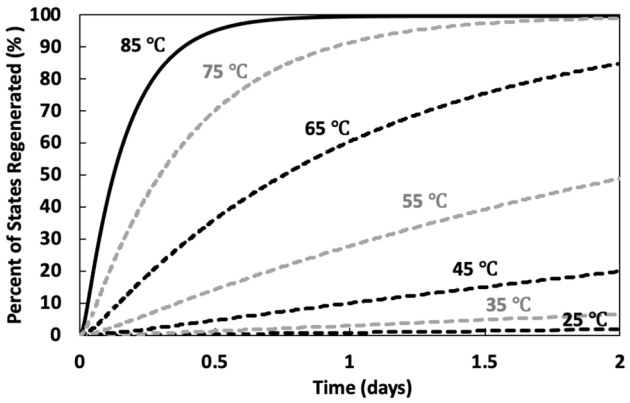

Fig. 5. Calculated percent of defects in regenerated state as a function of time, while applying Isc, at temperatures ranging from 25 °C to 85 °C.

potentially producing a false positive for a module that starts in state B. Thus, it is proposed that additional stabilization for BO LID be performed for accelerated stress sequences C, D and E, as shown in the underlined entries in Table 5. The proposed new stabilization is underlined where added to in Table 5. For sequences C and D, where thermal cycling can unintentionally regenerate degraded samples, the new stabilization would be performed only before stress. In sequence E, where samples regenerated at the manufacturer may destabilize in DH, the new stabilization would need to be performed both before and after stress. In each case, Gate 2 would be evaluated by comparing the post-stress measurement with the pre-stress (after stabilization) measurement. While this recommendation involves the addition of an extra *IV* measurement and up to two stabilization treatments for these sequences, it removes artifacts and uncertainty associated with BO LID defects, as can be seen in the final column of Table 5. The largest error anticipated due to BO LID is reduced to 1.8% relative and is limited to sequence C. The error occurs because the HF stress which is applied last in sequence C involves eight days at high temperature without current flow. These conditions destabilize ~ 20% of the defects. The addition of a second post stress stabilization before the final measurement would also remove this remaining error, which may be particularly important for extended (beyond IEC 61215) stress tests where multiple iterations of 10 HF cycles are applied consecutively.

It is important that the proposed stabilization is performed *after* Gate 1 is evaluated. Regeneration of BO LID impacts power generation of fielded modules over a non-negligible time period. For example, one study showed that modules fielded at their maximum power point for five weeks showed no sign of regeneration within this timeframe (Lee et al., 2015). Thus, Gate 1 nameplate verification must be performed before the proposed stabilization, which will drive all BO LID defects to regeneration.

The effect of the proposed stabilization on LeTID defects is shown in Table 6. For modules with defects in the initial state, the additional stabilization is expected to drive LeTID defects into the degraded state, with a fraction of those defects continuing to regeneration. For sequence E, which contains a second stabilization, some further regeneration occurs. As the LeTID regeneration is a relatively slow process however, the effects on Gate 2 evaluation are minimal. The largest error in Gate 2 due to LeTID is less than 1% relative, as shown in the final column of Table 6.

Thus, the results in Table 6 indicate that LeTID is unlikely to substantially impact the accuracy of Gate 2 evaluations with the addition of the proposed stabilization. However, this situation should continue to be monitored as the kinetics of LeTID become better documented with further studies. There also still remains the need for a LeTID test procedure to identify LeTID sensitive modules and quantify their degradation.

The proposed stabilization described in this section is currently

Table 5
Simulated defect status and apparent performance change for a module that exhibits 6% BO LID and no other degradation, for portions of a proposed modified IEC 61215 test proceeding.

At right is each step as module advances through the sequence:	B-O defect start-ing state	Defect status after MQT 19.1	Pre-stress stabil-ization	Defect status following stabil-ization	Stress 1	Defect status follow-ing stress 1	Stress 2	Defect status following stress 2	Final power, relative to pre-stress measure-ment (%)
IEC 61215 Sequence C	A	B	*85 °C, Isc, 48 hrs*	C	50 TC	1% B, 99% C	10 HF	11% A, 8% B, 81% C	(98.2 to) 99.2
	B	B	*85 °C, Isc, 48 hrs*	C	50 TC	1% B, 99% C	10 HF	11% A, 8% B, 81% C	(98.2 to) 99.2
	C	C	*85 °C, Isc, 48 hrs*	C	50 TC	1% B, 99% C	10 HF	11% A, 8% B, 81% C	(98.2 to) 99.2
IEC 61215 Sequence D	A	B	*85 °C, Isc, 48 h*	C	200 TC	99% C, 1% B	–	–	100
	B	B	*85 °C, Isc, 48 h*	C	200 TC	99% C, 1% B	–	–	100
	C	C	*85 °C, Isc, 48 h*	C	200 TC	99% C, 1% B	–	–	100
IEC 61215 Sequence E	A	B	*85 °C, Isc, 48 hrs*	C	DH	36% C, 5% B, 59% A	*85 °C, Isc, 48 hrs*	C	100
	B	B	*85 °C, Isc, 48 hrs*	C	DH	36% C, 5% B, 59% A	*85 °C, Isc, 48 hrs*	C	100
	C	C	*85 °C, Isc, 48 hrs*	C	DH	36% C, 5% B, 59% A	*85 °C, Isc, 48 hrs*	C	100
IEC 61215 Sequence F (planned)	A	B	*85 °C, Isc, 48 hrs*	C	PID	91% C, 6% B, 3% A	–	–	(99.0 to) 99.3
	B	B	*85 °C, Isc, 48 hrs*	C	PID	91% C, 6% B, 3% A	–	–	(99.0 to) 99.3
	C	C	*85 °C, Isc, 48 hrs*	C	PID	91% C, 6% B, 3% A	–	–	(99.0 to) 99.3
		↑ Gate 1 Measurement		↑ Pre-Stress Measurement				↑ Gate 2 Measurement	

Table 6
Simulated defect status and apparent performance change for a module that exhibits 6% LeTID and no other degradation, for portions of a proposed modified IEC 61215 test proceeding.

At Right is Each Step as Module Advances Through the Sequence:	LeTID Defect Starting State	Defect Status After MQT 19.1	Pre-Stress Stabil-ization	Defect Status Fol-lowing Stabil-ization	Stress 1	Defect Status Follow-ing Stress 1	Stress 2	Defect Status Following Stress 2	Final Power, Relative to Pre-Stress Measure-ment (%)
IEC 61215 Sequence C	Initial	Initial	*85 °C, Isc, 48 hrs*	82% degraded, 18% regenerated	50 TC	79% degraded, 21% regenerated	10 HF	79% degraded, 21% regenerated	100.1
	Degraded	Degraded	*85 °C, Isc, 48 hrs*	81% degraded, 19% regenerated	50 TC	79% degraded, 21% regenerated	10 HF	21% degraded, 21% regenerated	100.1
	Regenerated	Regenerated	*85 °C, Isc, 48 hrs*	100% regenerated	50 TC	100% regenerated	10 HF	100% regenerated	100
IEC 61215 Sequence D	Initial	Initial	*85 °C, Isc, 48 hrs*	82% degraded, 18% regenerated	200 TC	72% degraded, 28% regenerated	–	–	100.4
	Degraded	Degraded	*85 °C, Isc, 48 hrs*	81% degraded, 19% regenerated	200 TC	71% degraded, 29% regenerated	–	–	100.4
	Regenerated	Regenerated	*85 °C, Isc, 48 hrs*	100% regenerated	200 TC	100% regenerated	–	–	100
IEC 61215 Sequence E	Initial	Initial	*85 °C, Isc, 48 hrs*	82% degraded, 18% regenerated	DH	82% degraded, 18% regenerated	*85 °C, Isc, 48 hrs*	66% degraded, 35% regenerated	100.7
	Degraded	Degraded	*85 °C, Isc, 48 hrs*	81% degraded, 19% regenerated	DH	81% degraded, 19% regenerated	*85 °C, Isc, 48 hrs*	65% degraded, 35% regenerated	100.7
	Regenerated	Regenerated	*85 °C, Isc, 48 hrs*	100% regenerated	DH	100% regenerated	*85 °C, Isc, 48 hrs*	100% regenerated	100
IEC 61215 Sequence F (planned)	Initial	Initial	*85 °C, Isc, 48 hrs*	82% degraded, 18% regenerated	PID	82% degraded, 18% regenerated	–	–	100
	Degraded	Degraded	*85 °C, Isc, 48 hrs*	81% degraded, 19% regenerated	PID	81% degraded, 19% regenerated	–	–	100
	Regenerated	Regenerated	*85 °C, Isc, 48 hrs*	100% regenerated	PID	100% regenerated	–	–	100
		↑ Gate 1 Measurement		↑ Pre-Stress Measurement				↑ Gate 2 Measurement	

under consideration by the IEC 61215 project team.

The choice of appropriate stabilization depends on the duration and stress levels applied. Some tests apply several times the duration of stresses specified in IEC 61215. Examples of such longer tests include the proposed IEC TS 63209, "Extended-stress testing of photovoltaic modules for risk analysis," and similar test protocols developed by individual commercial test labs. Longer stress durations mean that the impacts of BO LID and LeTID may be different: The estimates of Table 3 through to Table 6 need to be recalculated for longer times. Appropriate stabilization may be different for shorter (e.g. IEC 61215) versus longer (e.g. IEC TS 63209) stress times and should be derived or verified with separate sets of calculations.

4. Conclusions

Finely tuned accelerated testing is the key to minimizing the occurrence of module failures in PV systems, and distinguishing between high-risk and low-risk products, to ensure economic viability of PV projects. The accelerated tests in IEC 61215 are widely used and have been developed over the years to screen for module failures. In this study, the expected impacts of BO LID and LeTID during IEC 61215 stress tests were estimated via simulation. Simulations were performed using published values of activation energies and attempt frequencies for defect reaction rates. Where such values are not available, or do not fully describe behavior during the relatively low-temperature stress tests, rates at 85 °C were extracted based on published data sets. It was found that BO LID may cause some false positives and false negatives when IEC 61215 tests are performed as prescribed in the 2016 published version. The errors introduced by BO LID can be corrected by additional stabilization steps. To stabilize, before stress in sequences containing thermal cycles, humidity-freeze, or damp heat (i.e. sequences C, D, and E), a current of I_{sc} should be applied to the module in the dark at 85 °C for 48 h. In sequence E (containing damp heat stress, the longest high-temperature exposure without injection), the same stabilization should also be applied after stress. Gate 2, the final module power evaluation for these sequences, would then compare power output just before stress

(after the first stabilization step) to the final power output. For a module with fairly large (6% relative) extent of BO LID or LeTID, the IEC 61215:2016 procedures can result in errors up to 6% relative. Use of the new stabilization in the test sequences limits artifacts to less than 2% relative. Appropriate stabilization may differ if stress duration is increased beyond that in IEC 61215, and thus stabilization for extended stress tests should be derived or verified with a separate set of calculations.

Declaration of Competing Interest

The authors declare that they have no known competing financial interests or personal relationships that could have appeared to influence the work reported in this paper.

Acknowledgements

The authors thank the IEC 61215 project team for discussions related to stabilization, LeTID, and BO LID. This work represents a collaboration among authors supported by different programs. Work at Hanwha Q CELLS GmbH is supported in part by the German ministry of Economy WIPANO grant "LeTID-Norm", FKZ 03TNH021E. Work at UNSW is supported in part by the Australian Research Council through a Discovery Early Career Researcher Award (DE170100620). This work was authored in part by the National Renewable Energy Laboratory, operated by Alliance for Sustainable Energy, LLC, for the U.S. Department of Energy (DOE) under Contract No. DE-AC36-08GO28308. This material is based upon work supported by the U.S. Department of Energy's Office of Energy Efficiency and Renewable Energy (EERE) under Solar Energy Technologies Office (SETO) Agreement Number 34357. The views expressed in the article do not necessarily represent the views of the DOE or the U.S. Government. The U.S. Government retains and the publisher, by accepting the article for publication, acknowledges that the U.S. Government retains a nonexclusive, paid-up, irrevocable, worldwide license to publish or reproduce the published form of this work, or allow others to do so, for U.S. Government Purposes. The authors also thank Itai Suez of Silfab Solar, Tristan Erion-Lorico of PVEL, and Cherif Kedir and Zen Villanueva of RETC for providing supplementary industrial data that help illustrate the need for this study.

References

Bothe, K., Schmidt, J., 2006. Electronically activated boron-oxygen-related recombination centers in crystalline silicon. J. Appl. Phys. 99, 013701.
Bothe, K., Sinton, R., Schmidt, J., 2005. Fundamental boron-oxygen-related carrier lifetime limit in mono-and multicrystalline silicon. Prog. Photovolt. Res. Appl. 12, 287–296.
Bredemeier, D., Walter, D.C., Heller, R., Schmidt, J., 2019. Impact of hydrogen-rich silicon nitride material properties on light-induced lifetime degradation in multicrystalline silicon. Phys. Status Solidi RRL 13, 1900201.
Bredemeier, D., Walter, Dominic, Schmidt, Jan, 2017. Light-induced lifetime degradation in high-performance multicrystalline silicon: Detailed kinetics of the defect activation. Sol. Energy Mater. Sol. Cells 173, 2–5.
Chang, N.L., Ho-Baillie, A., Wenham, S., Woodhouse, M., Evans, R., Tjahjono, B., Qi, F., Chong, C.M., Egan, R.J., 2018. A techno-economic analysis method for guiding research and investment directions for c-Si photovoltaics and its application to Al-BSF, PERC, LDSE and advanced hydrogenation. Sustainable Energy Fuels 2, 1007–1019.
Chen, D., et al., 2017. Evidence of an identical firing-activated carrier-induced defect in monocrystalline and multicrystalline silicon. Sol. Energy Mater. Sol. Cells 172, 293–300.
Chen, D., et al., 2018. Hydrogen induced degradation: A possible mechanism for light- and elevated temperature- induced degradation in n-type silicon. Sol. Energy Mater. Sol. Cells 185, 174–182.
Colville, F., 2017. "Mono and multi production 50:50 in 2018, but mono is the future" PVTECH Magazine, May 09, 2017, https://www.pv-tech.org/editors-blog/mono-and-multi-production-5050-in-2018-but-mono-is-the-future.
Deceglie, Michael G., Silverman, Timothy J, Johnston, Steve W., Rand, James A., Reed, Mason J., Flottemesch, Robert, Repins, Ingrid L., 2020. Light and elevated temperature induced degradation (LeTID) in a utility-scale photovoltaic system. IEEE J. Photovoltaics 10 (4), 1084–1092. https://doi.org/10.1109/JPHOTOV.550386910.1109/JPHOTOV.2020.2989168.
Deceglie, M.G., Silverman, T.J., Marion, B., Kurtz, S.R., 2015. Robust measurement of thin-film photovoltaic modules exhibiting light-induced transients. Proc. SPIE - The Int. Soc. Opt. Eng. 9561, 956108.
Fertig, F., Broisch, J., Biro, D., Rein, S., 2014. Stability of the regeneration of the boron–oxygen complex in silicon solar cells during module certification. Sol. Energy Mater. Sol. Cells 121, 157–162.
Fiorentini, L., Marmo, L., Danzi, E., Puccia, V., 2016. Fire risk assessment of photovoltaic plants. A case study moving from two large fires: From accident investigation and forensic engineering to fire risk assessment for reconstruction and permitting purposes. Chem. Eng. Trans. 48, 427–432.
Fischer, H., Pschunder, W., 1973. Investigation of photon and thermal induced changes in silicon solar cells. Proc. IEEE PVSC 10, 404–411.
Fokuhl, E., et al., 2019. LeTID – A comparison of test methods on module level. In: 36th European Photovoltaic Solar Energy Conference and Exhibition, pp. 816–821.
Gläser, M., Lausch, D., 2015. Towards a quantitative model for BO regeneration by means of charge state control of hydrogen. Energy Procedia 77, 592–598.
Glunz, S.W., Schaffer, E., Rein, S., Bothe, K., Schmidt, J., 2003. Analysis of the defect activation in Cz-silicon by temperature-dependent bias-induced degradation of solar cells. Proceedings of the World Conference on Photovoltaic Energy Conversion 3, 919–922.
Graf, A., Herguth, A., Hahn, G., 2019. Determination of BO-LID and LeTID related activation energies in Cz-Si and FZ-Si using constant injection conditions. AIP Conf. Proc. 2147, 140003.
Green, M.A., 1982. Solar Cells: Operating Principles, Technology, and System Applications. Prentice-Hall, Englewood Cliffs NJ equation 5.15, 96.
Hallam, B., Herguth, A., Hamer, P., Nampalli, N., Wilking, S., Abbott, M., Wenham, S., Hahn, G., 2018. Eliminating light-induced degradation in commercial p-type czochralski silicon solar cells. Appl. Sci. 8, 10. https://doi.org/10.3390/app8010010.
Hallam, B., et al., 2016. Modelling kinetics of the boron-oxygen defect system. Energy Procedia 92, 42–51.
Hashigami, H., Itakura, Y., Saitoh, T., 2003. Effect of illumination conditions on Czochralski-grown silicon solar cell degradation. J. Appl. Phys. 93, 4240–4245.
Helmich, L., et al., 2018. In-situ characterization of electron-assisted regeneration of Cz-Si solar cells. Sol. Energy Mater. Sol. Cells 185, 283–286.
Herguth, A., Derricks, C., Keller, P., Terheiden, B., 2017. Recovery of LeTID by low -intensity illumination: Reaction kinetics, completeness, and threshold temperature. Energy Procedia 124, 740–744.
Herguth, A., Hahn, G., 2010. Kinetics of the boron-oxygen related defect in theory and experiment. J. Appl. Phys. 108, 114509.
Herguth, A., Schubert, G., Kaes, M., Hahn, G., 2006. Avoiding boron-oxygen related degradation in highly boron doped CZ silicon. In: 21st European Photovoltaic Solar Energy Conference and Exhibition, pp. 530–537.
Herguth, A., Schubert, G., Kaes, M., Hahn, G., 2008. Investigations on the long time behavior of the metastable boron-oxygen complex in crystalline silicon. Prog. Photovolt: Res. Appl. 16, 135–140.
Hieslmair, H., 2017. Time constants of degradation, regeneration, and destabilization of the B-O related defect. Proceedings of the IEEE Photovoltaic Specialist Conference 44, 1–6.
IEC 61215-1, IEC 61215-2, IEC 61215-1-1, IEC 61215-1-2, IEC 61215-1-3, IEC 61215-1-4 at https://webstore.iec.ch/searchform&q=IEC%2061215.
Jensen, M.A., Morishige, A.E., Hofstetter, J., Needleman, D.B., Buonassisi, T., 2017. Evolution of LeTID defects in p-type multicrystalline silicon during degradation and regeneration. IEEE J. Photovoltaics 7 (4), 980–987.
Kenny, R.P., Chatzipanagi, A.I., Sample, T., 2014. Preconditioning of thin-film PV module technologies for calibration. Prog. Photovoltaics Res. Appl. 22 (2), 166–172.
Kersten, F., et al., 2017. System performance loss due to LeTID. Energy Procedia 124, 540–546.
Kersten, F., et al., 2019. Stability investigations of Cz-PERC modules during damp heat testing and transport: the impact of the boron-oxygen defect. AIP Conf. Proc. 2147, 090001.
Kersten, F., et al., 2015. Degradation of multicrystalline silicon solar cells and modules after illumination at elevated temperature. Sol. Energy Mater. Sol. Cells 142, 83–86.
Knobloch, J., et al., 1996. Solar cells with efficiencies above 21% processed from Czochralski grown silicon. IEEE Photovoltaic Specialists Conference 25, 405–408.
Kwapil, Wolfram, Niewelt, Tim, Schubert, Martin C., 2017. Kinetics of carrier-induced degradation at elevated temperature in multicrystalline silicon solar cells. Sol. Energy Mater. Sol. Cells 173, 80–84. https://doi.org/10.1016/j.solmat.2017.05.066.
Laidler, K.J., 1984. The development of the Arrhenius equation. J. Chem. Educ. 61, 494–498.
Lee, K., et al., 2015. Natural recovery from LID: Regeneration under field conditions?. In: In: 31st European Photovoltaic Solar Energy Conference and Exhibition, pp. 1837–1841.
Lim, B., Liu, A., Macdonald, D., Bothe, K., Schmidt, J., 2009. Impact of dopant compensation on the deactivation of boron-oxygen recombination centers in crystalline silicon. Appl. Phys. Lett. 95, 232109.
Lin, C.-M., et al., 2017. Accelerated light-induced degradation test for industrial application. In: 33rd European Photovoltaic Solar Energy Conference and Exhibition, pp. 978–982.
Liu, S., et al., 2018. Impact of dark annealing on the kinetics of light and elevated-temperature-induced degradation. IEEE J. Photovoltaics 8 (6), 1494–1502.
Luka, T., Turek, M., Hagendorf, C., 2018. Defect formation under high temperature dark-annealing compared to elevated temperature light soaking. Sol. Energy Mater. Sol. Cells 187, 194–198.

Mateo, C., Hernández-Fenollosa, M.A., Montero, Á., Seguí-Chilet, S., 2018. Analysis of initial stabilization of cell efficiency in amorphous silicon photovoltaic modules under real outdoor conditions. Renewable Energy 120, 114–212.
Müller, M., Ehrl, M., Heitmann, J., 2018. Energy yield considerations based on the BO-related defect. AIP Conf. Proc. 1999, 090002.
Niewelt, T., Schon, J., Warta, W., Glunz, S.W., Schubert, M.C., 2017. Degradation of crystalline silicon due to boron-oxygen defects. IEEE J. Photovoltaics 7 (1), 383–398.
Osterwald, C.R., McMahon, T.J., 2009. History of accelerated and qualification testing of terrestrial photovoltaic modules: a literature review. Prog. Photovolt: Res. Appl. 17, 11–33.
Payne, D.N.R., et al., 2016. Rapid passivation of carrier-induced defects in p-type multi-crystalline silicon. Sol. Energy Mater. Sol. Cells 158, 102–106.
Peters, I.M., Rodriguez Gallegos, C.D., Sofia, S.E., Buonassisi, T., 2019. The value of efficiency in photovoltaics. Joule 3, 2732–2747.
Pickerel, K., "Solar's silent killer: Backsheets are shortening some project lifespans," Solar Power World, January 15, 2020. https://www.solarpowerworldonline.com/2020/01/solars-silent-killer-backsheets-are-shortening-project-lifespans/.
Pingel, S., et al., 2010. Initial degradation of industrial silicon solar cells in solar panels. In: 25th European Photovoltaic Solar Energy Conference and Exhibition, pp. 4027–4032.
Ross, R.G. Jr., M.I. Smokler, "Electricity from Photovoltaic Solar Cells : Flat-Plate Solar Array Project Final Report : 11 years of Progress, October 1986," Government report "JPL Publication 86-31," 1986.
Ramspeck, K., et al., 2012. Light induced degradation of rear passivated mc-Si solar cells. In: 27th European Photovoltaic Solar Energy Conference and Exhibition, pp. 861–865.
Runkle, L.D., Dumas, L.N., 1980. Progress in the performance of terrestrial solar cell modules. In: Proceedings of the 1980 Annual Meeting of the American Section of the International Solar Energy Society, pp. 1109–1113.
Sio, H.C., et al., 2018. Light and elevated temperature induced degradation in p-type and n-type cast-grown multicrystalline and mono-like silicon. Sol. Energy Mater. Sol. Cells 182, 98–104.
Smokler, M.I. D.H. Otth, R.G. Ross, Jr., "The Block Program Approach to Photovoltaic Module Development," Proceedings of the IEEE Photovoltaic Specialists Conference 18, 1985, pp. 1150-1158.
Steckenreiter, V., Walter, D.C., Schmidt, J., 2017. Kinetics of the permanent deactivation of the boron-oxygen complex in crystalline silicon as a function of illumination intensity. AIP Adv. 7, 035305.
Sun, C., et al., 2019. Kinetics and dynamics of the regeneration of boron-oxygen defects in compensated n-type silicon. Sol. Energy Mater. Sol. Cells 195, 174–181.
Vargas, C., Coletti, G., Chan, C., Payne, D., Hameiri, Z., 2019. On the impact of dark annealing and room temperature illumination on p-type multicrystalline silicon wafers. Sol. Energy Mater. Sol. Cells 189, 166–174.
Wilking, S., Das Wasserstoff-Modell der Bor-Sauerstoff-Regeneration, Ph.D. dissertation, Dept. of Physics, Univ. Konstanz, Konstanz, Baden-Württemberg, Germany, 2017. See chapter 4.1.1.
Wilking, S., Beck, C., Ebert, S., Herguth, A., Hahn, G., 2014. Influence of bound hydrogen states on BO-regeneration kinetics and consequences for high-speed regeneration processes. Sol. Energy Mater. Sol. Cells 131, 2–8.
Wilking, S., Forster, M., Herguth, A., Hahn, G., 2015. From simulation to experiment: Understanding BO-regeneration kinetics. Sol. Energy Mater. Sol. Cells 142, 87–91.
Wohlgemuth, J., 2011. History of IEC qualification standards, Government report NREL/PR-5200-52246.
Yang, H., Wang, F., Wang, H., Chang, J., Song, D., Su, C., 2017. Performance deterioration of p-type single crystalline silicon solar modules affected by potential induced degradation in photovoltaic power plant. Microelectron. Reliab. 72, 18–23.